

# Vertically Oriented Carbon Nanostructures and Their Application Potential for Polymer-Based Solar Cells

Holger Borchert,<sup>\*,†</sup> Florian Witt,<sup>†</sup> Alina Chanaewa,<sup>‡</sup> Fabian Werner,<sup>§</sup> Jan Dorn,<sup>§</sup> Thomas Dufaux,<sup>||</sup> Marta Kruszynska,<sup>†</sup> Anne Jandke,<sup>†</sup> Michael Höltig,<sup>‡</sup> Tamara Alfere,<sup>§</sup> Jens Böttcher,<sup>‡</sup> Christoph Gimmmer,<sup>§</sup> Christian Klinke,<sup>‡</sup> Marko Burghard,<sup>||</sup> Alf Mews,<sup>‡</sup> Horst Weller,<sup>‡</sup> and Jürgen Parisi<sup>†</sup>

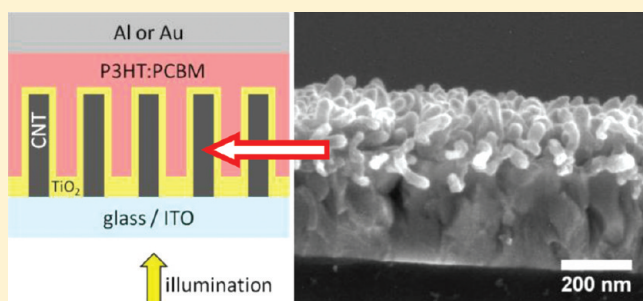
<sup>†</sup>University of Oldenburg, Department of Physics, Energy and Semiconductor Research Laboratory, Carl-von-Ossietzky-Str. 9-11, 26129 Oldenburg, Germany

<sup>‡</sup>University of Hamburg, Institute of Physical Chemistry, Grindelallee 117, 20146 Hamburg, Germany

<sup>§</sup>Center of Applied Nanotechnology (CAN) GmbH, Grindelallee 117, 20146 Hamburg, Germany

<sup>||</sup>Max Planck Institute for Solid State Research, Heisenbergstraße 1, 70569 Stuttgart, Germany

**ABSTRACT:** One factor limiting the performance of polymer-based bulk heterojunction solar cells is inefficient charge transport in the disordered donor/acceptor blends. The incorporation of carbon nanotubes (CNTs) into the active layer is considered as a promising concept to improve charge transport toward the electrodes. Whereas disordered ternary blends of polymer, fullerenes and CNTs, were already examined in the past, there is much less work on ordered vertically oriented arrays of nanotubes for solar cell applications. We focused on the fabrication of corresponding arrays with spatial dimensions that are suitable for application in polymer-based solar cells. We demonstrate in this contribution that CNTs can be grown on ITO covered glass at temperatures below 600 °C by static pressure chemical vapor deposition (CVD). Using short growth times, we were able to obtain CNT arrays with a rather uniform length limited to about 200 nm. With a plasma-enhanced CVD process, we were also able to produce wall-like carbon nanostructures (multilayered graphene sheets) with controllable height on ITO. Both types of carbon nanostructures were investigated in test solar cells, in order to explore their suitability for application in organic photovoltaics. Efficiencies remained low so far ( $\sim 0.2\%$ ), but the successful incorporation of the new ordered structures into solar cells could be demonstrated, and issues for further optimization are discussed.



## 1. INTRODUCTION

Polymer-based solar cells are a promising technology for the fabrication of low-cost photovoltaic devices. A widely used concept is so-called bulk heterojunction (BHJ) solar cells where a blend of two materials, e.g., an organic polymer/fullerene or an organic–inorganic polymer/nanoparticle blend, is placed as the active layer between two electrodes.<sup>1–4</sup> With suitable offsets between the energy levels of the highest occupied molecular orbital (HOMO) and lowest unoccupied molecular orbital (LUMO), the blend forms a donor/acceptor system which is suitable to separate photogenerated electron–hole pairs at the interface. One of the most widely examined material systems consists of poly(3-hexylthiophene) (P3HT) as electron donor and [6,6]-phenyl-C<sub>61</sub>-butyric acid methyl ester (PCBM) as electron acceptor. Compared to inorganic devices, the efficiency of polymer-based solar cells remains limited, so far. The highest efficiencies reported to date for organic BHJ solar cells reach 6–8%,<sup>5–7</sup> although efficiencies exceeding 10% should be possible with single junction BHJ solar cells according to theoretical considerations.<sup>8</sup>

One of the main problems causing efficiency losses is the inefficient charge transport in the disordered bulk heterojunction of polymer/fullerene solar cells. Many studies were devoted to the characterization and optimization of morphology of organic BHJ layers.<sup>9–12</sup> In the case of organic–inorganic P3HT/ZnO blends, electron tomography studies even enabled the visualization of the three-dimensional networks of the two material components in the blends.<sup>13</sup> The presence of isolated domains of one material as well as dead ends was observed.<sup>13</sup> Both of these structural features are a clear obstacle for efficient charge transport toward the electrodes.

One strategy to improve charge transport in BHJ solar cells is the incorporation of carbon nanotubes (CNTs) into the active layer. Many studies in this field discuss single-walled CNTs to act as electron acceptors which shall help to transport electrons efficiently to the cathode.<sup>14–17</sup> However, other reports state that

**Received:** October 4, 2011

**Revised:** November 24, 2011

**Published:** December 06, 2011

single-walled CNTs can also act as hole acceptors,<sup>18</sup> and there are also many works, where single-walled CNT networks are used as hole-collecting electrode.<sup>19,20</sup> Metallic, multiwalled CNTs having a work function of the order of  $\sim 5$  eV were also investigated as additives to polymer/fullerene solar cells and discussed to act as hole acceptors.<sup>21</sup> Whereas some reports stated a positive effect of incorporating CNTs into BHJ blends,<sup>15,21</sup> other studies came to different conclusions. For example, Derbal-Habak et al.<sup>17</sup> recently found that the addition of small amounts of single-walled CNTs to P3HT/PCBM BHJ solar cells increases the device performance only in the case of nonannealed films. An impact on molecular order in the P3HT phase was discussed to be responsible for this improvement rather than enhanced electron transport. After annealing, CNT-free reference cells showed the best performance in that study.<sup>17</sup> Thus, it is still under discussion if CNTs added to a BHJ blend can really have a positive influence due to improved charge transport.

Instead of simply adding CNTs to a BHJ blend, the fabrication of vertically ordered CNT arrays appears more promising. CNT arrays with dimensions in the micrometer size regime were already successfully prepared and for example demonstrated by Liu et al.<sup>22</sup> to be relevant structures for dye-sensitized solar cells. However, efficiencies were limited to about 1% in the corresponding work.<sup>22</sup> In polymer/fullerene solar cells, the typical active layer thickness is only a few hundreds of nanometers. Miller et al.<sup>23</sup> prepared approximately 200 nm long multiwalled CNTs on indium tin oxide (ITO) and studied the structures as interpenetrating, hole-collecting electrodes in organic solar cells. Although the CNTs were concluded to have a positive effect on the hole collection efficiency, the overall device performance was lower as compared to CNT-free reference solar cells in that work, because the CNTs resulted in reduced transparency of the electrode and in a reduced fill factor.<sup>23</sup>

In the present work, we used different chemical vapor deposition (CVD) processes to develop elongated carbon nanostructures vertically oriented on indium tin oxide (ITO) with advanced control over the length in the size regime of about 100 nm which appears relevant for polymer/fullerene solar cells. Experiments on the application of these carbon nanostructures in solar cells are presented as well. For further comparison, we also studied the incorporation of multiwalled CNTs into disordered polymer/fullerene/CNT BHJ solar cells.

## 2. EXPERIMENTAL SECTION

Arrays of carbon nanotubes (CNTs) were grown on ITO by CVD as follows: the ITO substrates were structured, cleaned in ultrasonic bath with acetone followed by ethanol and treated with oxygen plasma for 20 min to remove organic residues. Five nm thick iron film was evaporated onto the cleaned substrates. Subsequently, the substrates were inserted into a steady-state reactor. After evacuation of the chamber to  $10^{-4}$  mbar, 10 mbar of acetylene were let in. The temperature was increased up to 575 °C. To produce 200 nm long tubes, temperature was decreased immediately after reaching 575 °C, whereas for  $\sim 5 \mu\text{m}$  long ones the reaction time was extended to 10 min.

Titania hole blocking layers were deposited on the CNTs via spin coating of tetraethylorthotitanate in isopropyl alcohol (1:100) at 1000 rpm for 40 s. Subsequently, the samples were annealed at 100 °C in air. This procedure was repeated up to six times. The final spin coating step was followed by heating at 475 °C in a vacuum oven.

Arrays of carbon nanowalls (CNWs) were fabricated on ITO substrates by using a custom-built plasma-enhanced CVD setup (PECVD) from a mixture of C<sub>2</sub>H<sub>2</sub>, H<sub>2</sub>, and Ar. The PECVD system resembles a parallel plate RF (13.56 MHz) capacitively coupled plasma (CCP) with C<sub>2</sub>H<sub>2</sub> as carbon source and a resistively heatable stage acting both as counter electrode and substrate holder. The C<sub>2</sub>H<sub>2</sub>, H<sub>2</sub>, and Ar flow rates were maintained at 20, 70, and 70 standard cubic centimeters (sccm), respectively. The plasma power was 20 W and the reaction was carried out for 20 min at 500 °C while the total pressure was kept at 20 mbar.

Conductivity studies of individual titania-coated CNTs were performed as follows: 1.5 mg multiwalled CNTs („Baytubes“ purchased from Bayer) were sonicated in 1 mL ethanol for 2 h and subsequently introduced into 22 mL of ethanol solution containing 77 μL of titanium-*n*-butoxide (TBOT) and 144 μL of water. This mixture was heated at reflux for 90 min. After cooling the reaction mixture, the composite material was precipitated by adding *n*-heptane, and it was washed with ethanol twice. This synthetic procedure was adapted from the coating procedure for Stöber silica spheres published by Hanprasopwattana et al.<sup>24</sup>

Solar cells with multiwalled CNTs added to disordered BHJ blends were prepared as follows: Cleaned ITO-coated glass substrates were covered by spin-coating with a layer of poly(3,4-ethylenedioxythiophene):poly(4-styrenesulfonate) (PEDOT:PSS, formulation Clevios P VP AI 4083, purchased from H. C. Starck). The substrates were then transferred into a nitrogen-filled glovebox, where the active layer consisting of blends of P3HT (purchased from Rieke Metals), PCBM (purchased from Solenne BV) and optionally multiwalled CNTs („Baytubes“ obtained from Bayer) was deposited by spin-coating. Chlorobenzene was used as solvent. The weight ratio of P3HT:PCBM was kept constant at 1:1, and the total concentration of the solutions used for spin-coating was 10 mg/mL. CNTs were optionally added in relatively high concentration in the weight ratio of 1:2:2 CNTs:P3HT:PCBM. The active layer thickness resulting from the preparation by spin-coating was in the range of 100 - 200 nm. Subsequently, the samples were annealed to 140 °C for 10 min, before an Al electrode was thermally evaporated on top of the active layer. The active area of these solar cells was approximately 0.1 cm<sup>2</sup>.

Prior to using the CNTs, their surface was functionalized as follows: 10 mg of pure MWCNTs were dispersed in a mixture of nitric and sulfuric acids (5 mL, HNO<sub>3</sub>:H<sub>2</sub>SO<sub>4</sub> = 1:3, v:v). Next, the suspension was optionally sonicated for 6 h at 50 °C. After centrifugation, the residue was washed several times with deionized water until the pH value of the filtrate was 7, and the modified MWCNTs were suspended in chlorobenzene. With the introduction of the optional sonication step, not only the surface of CNTs was modified, but additionally their length was shortened. Typically, the length of the initial CNTs was on the level of several micrometers, whereas after the treatment it was below 1  $\mu\text{m}$ , with an average length around 200 nm.

Solar cells based on ordered carbon nanostructures were prepared as follows: The substrates with the carbon nanostructures on ITO were infiltrated with solutions of P3HT:PCBM (1:1 wt:wt) in chlorobenzene inside a nitrogen-filled glovebox. The concentration of the solution was 10 mg/mL. Therefore, either spin-coating or simply drop casting was used. Afterward, the films were annealed to 140 °C for 10 min. Finally, a metal electrode of Al or Au was thermally evaporated on top of the active layer.

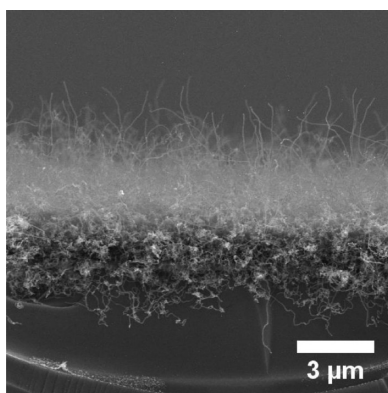


**Figure 1.** Scanning electron microscope image of carbon nanotubes grown on ITO-coated glass for 10 min in a static pressure CVD reactor using 10 mbar of acetylene at 575 °C.

Characterization of the solar cells was done by current–voltage measurements. Therefore, solar simulators were used. We used either a PET triple A SS80AAA solar simulator in combination with a Keithley 2400 sourcemeter, or a solar simulator LOT-Oriel LS0306 in combination with an Agilent 4156C parameter analyzer. The cells were illuminated with 100 mW/cm<sup>2</sup> simulated AM 1.5 radiation. Spectral mismatch was not taken into account.

### 3. RESULTS AND DISCUSSION

**3.1. Carbon Nanostructures.** In order to establish novel types of solar cells which involve nanostructures, be it carbon nanotubes or inorganic nanoparticles, it is desirable to establish the layered composite structure on a transparent, inexpensive but conductive material. A suitable choice is indium–tin oxide (ITO) covered aluminum silicate glass. The method of choice to produce carbon nanotube films directly on conductive substrates is chemical vapor deposition (CVD). Usually, carbon nanotubes are grown at temperatures between 650 and 800 °C using acetylene as carbon source and a transition metal as catalyst. Unfortunately, silicate glasses start to soften at 666 °C (strain point).<sup>25</sup> There are only a few examples of successful growth of carbon nanotubes on glass or ITO.<sup>23,26</sup>

In the present work, we used a CVD reactor with a boron nitride heating plate under a static acetylene pressure. This setup is heating the sample and not the whole acetylene atmosphere. Acetylene gets thermalized in the moment when the molecules reach the catalyst. First, we evacuated the chamber to a base pressure of 10<sup>-4</sup> mbar. Then, we introduced an acetylene pressure of 10 mbar followed by heating the sample to a temperature of 575 °C. The samples were covered with a thermally evaporated iron film of nominally 5 nm thickness. Upon heating this layer forms grains in the order of a few nanometers which act as catalyst. The introduction of acetylene before the heating has the advantage of being more controllable than the introduction when the growth temperature is already reached. At temperatures of 600 °C and higher, ITO gets reduced by the acetylene and indium segregates which leads to unwanted structures on the surface. Also the conductivity of the remaining ITO is reduced by 1–2 orders of magnitude due to the indium loss. At temperatures between 500 and 575 °C, we observed a growth of carbon nanotubes without softening of the glass or harming the ITO. The diameter and the diameter distribution (polydispersity) of the

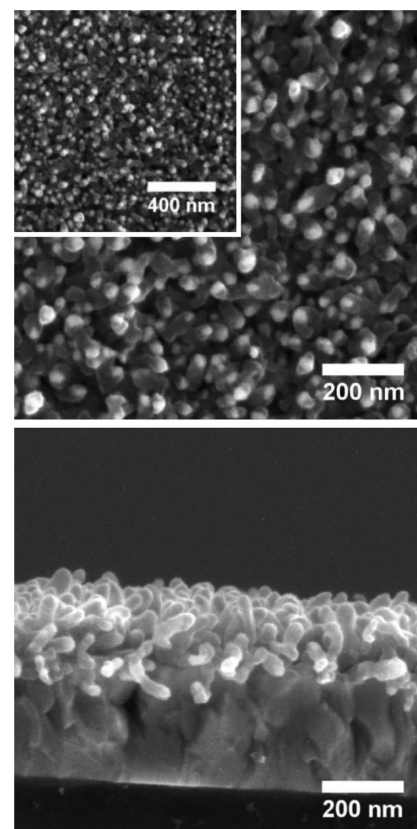


**Figure 2.** Scanning electron microscope images (top view and side view) of carbon nanotubes grown on ITO-coated glass in a static pressure CVD reactor with 10 mbar acetylene applying a very limited growth period. The bright spots visible in the high magnification top view image are the catalyst particles in the head of the tubes.

CNT's increase with decreasing temperature. Thus, we reach an optimum at 575 °C where, using a growth time of 10 min, pure carbon nanotubes form with a diameter of 24 ± 3 nm (Figure 1). The length of the tubes varies and is in the order of 3 μm. This is, however, too long for application in polymer/fullerene solar cells, because the carbon structure would establish a direct contact between the electrodes and thus induce electrical shorts.

In order to reduce the length of the tubes we decreased the growth period at 575 °C from 10 min to virtually 0 min, meaning the substrate holder was heated and the heating was immediately switched off after reaching growth temperature of 575 °C. This resulted in carbon nanotubes of uniform 200 nm in length (Figure 2). Note that obtaining a uniform length is not trivial. Usually, nanotubes start to grow at a random point in time after reaching the growth temperature. The catalyst grains need a certain activation period to establish an oversaturation with catalytically decomposed carbon.<sup>27</sup> Also the poisoning of the catalyst which is responsible for the cease of the growth by e.g. a complete amorphous carbon layer around the catalyst grains is not controlled and thus, the length of the tubes is usually not predetermined.

If the CNTs have metallic character, they are on the one hand supposed to improve the transport of one type of charge carriers to the electrode, but on the other hand, they can give rise to additional recombination events, when the other type of charge carriers reaches the CNTs. A strategy to avoid undesired recombination

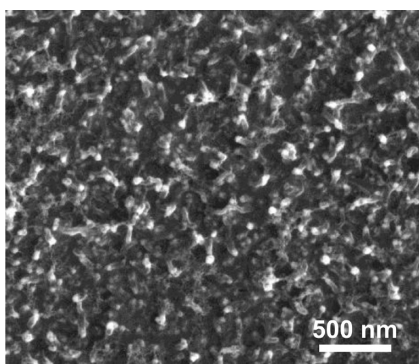


**Figure 3.** Scanning electron microscope image of  $\sim 200$  nm long carbon nanotubes coated with  $\text{TiO}_2$ . The titania layer was applied using 6 deposition/annealing cycles.

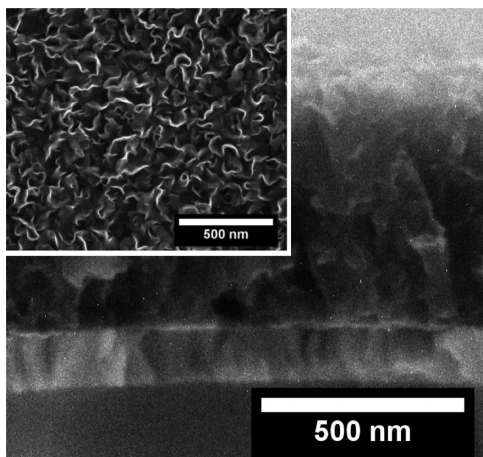


**Figure 4.** Cross-sectional SEM image of a CNW film grown on an ITO substrate using  $\text{C}_2\text{H}_2/\text{H}_2/\text{Ar}$ . For clarity the image shows an optically opaque, 600 nm thick CNW film which was grown within 2 h. Optically transparent CNW films used within solar cell device were grown for 20 min had a layer thickness of  $\sim 100$  nm. The inset shows the corresponding SEM top-view image.

is to coat the CNTs with an electron or hole blocking layer. For example, Liu et al.<sup>22</sup> used titania-coated multiwalled CNT arrays (with tube lengths in the micrometer size regime) in dye-sensitized solar cells to selectively collect electrons. We also established a method to coat our CNT structures with titania by thermal decomposition of tetraethylorthotitanate which was deposited on the CNT structures by spin-coating. The hole blocking layer was applied in several deposition/annealing cycles, in order to reach a good coverage of the CNTs. Figure 3 shows a typical scanning electron microscopy image of a titania-coated CNT array on ITO.

As an alternative to carbon nanotubes, we also used vertically aligned multilayer graphene sheets, named carbon nanowalls (CNWs) in the following. Therefore, a low temperature synthesis based on a plasma-enhanced CVD process was elaborated in order to grow CNW layers. CNW growth was carried out directly on ITO substrates and without further catalysts at temperatures as low as  $500^\circ\text{C}$ . It was found that for moderate reaction times (20 min) the resulting CNW layer thickness was around 100 nm. Figure 4 shows typical SEM images of the obtained CNW structures.

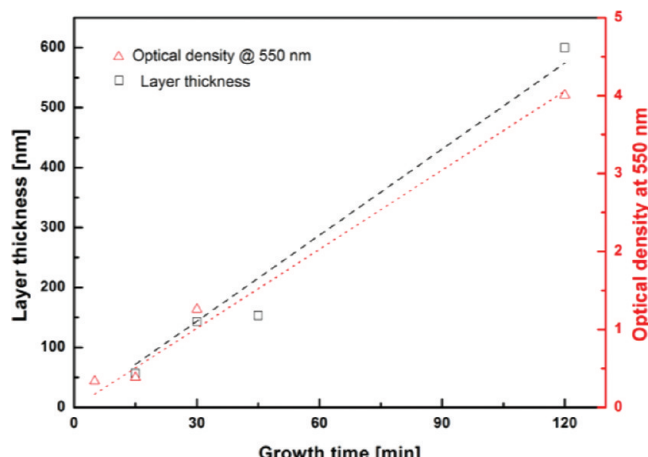


**Figure 5.** Optical density (red triangles) and layer thickness (black squares) of CNW film grown on ITO as a function of growth time.

In regard to photovoltaic applications of the carbon nanostructures on ITO, it is important that the samples remain partly transparent, at least, if the light will be coupled in from the ITO side. Therefore, we examined the layer thickness and absorbance of the CNWs on ITO as a function of growth time. As can be seen from Figure 5 (black line), the CNW layer thickness linearly depends on growth time with a growth rate of  $\sim 290$  nm/hour. At the same time there is a linear dependence between the optical density at 550 nm and growth time. This enables us to carefully tune the samples degree of transparency during synthesis.

A CNW layer of 100–200 nm thickness attenuates the sunlight at 550 nm wavelength (corresponding to high absorption of P3HT) approximately to  $1/e$ . This means that corresponding CNW structures can be used for solar cells to be illuminated from the ITO side, but device concepts with illumination through the other electrode may be more promising.

**3.2. Conductivity.** When considering the use of carbon nanotubes as highly conductive elements to collect charge carriers within solar cells, care must be taken that their  $\text{sp}^2$ -bonded carbon framework remains intact, as this would otherwise deteriorate the excellent carrier mobility in these nanostructures. It is hence an important task to check the conductivity of the nanotubes after their decoration with a transition metal oxide. To this end, we have deposited the  $\text{TiO}_2$ -coated CNTs from dispersion in an organic solvent, followed by using e-beam lithography to define gold contacts ( $\text{Ti}/\text{Au}$  0.3/30 nm) onto individual tubes (see Figure 6a). In order to achieve good electrical contacts, it is necessary to locally remove the oxide shell around the nanotube. Due to the chemical inertness of  $\text{TiO}_2$ , this task turned out to be quite difficult. In fact, many etchants like hot sulfuric acid,<sup>28</sup> hydrofluoric acid,<sup>28</sup> or sputtering<sup>29</sup> are prone to destroy or at least partially damage the underlying nanotube, in particular since it is almost impossible to stop the etching process right in time. Note that direct evaporation of Au onto the oxide-coated tubes resulted in quasi-insulating behavior. As a possible workaround, we first evaporated the gold onto the oxide-coated tube (see Figure 6b), and subsequently performed an annealing step ( $370^\circ\text{C}$  for 15 min in argon atmosphere). The aim of this treatment was to (partially) melt the thin metal layer, such that gold atoms are able to diffuse through the oxide shell. The annealing caused a notable deformation of the gold contacts, as apparent from the AFM image in Figure 6a, suggestive of (partial) alloying of the metal into the

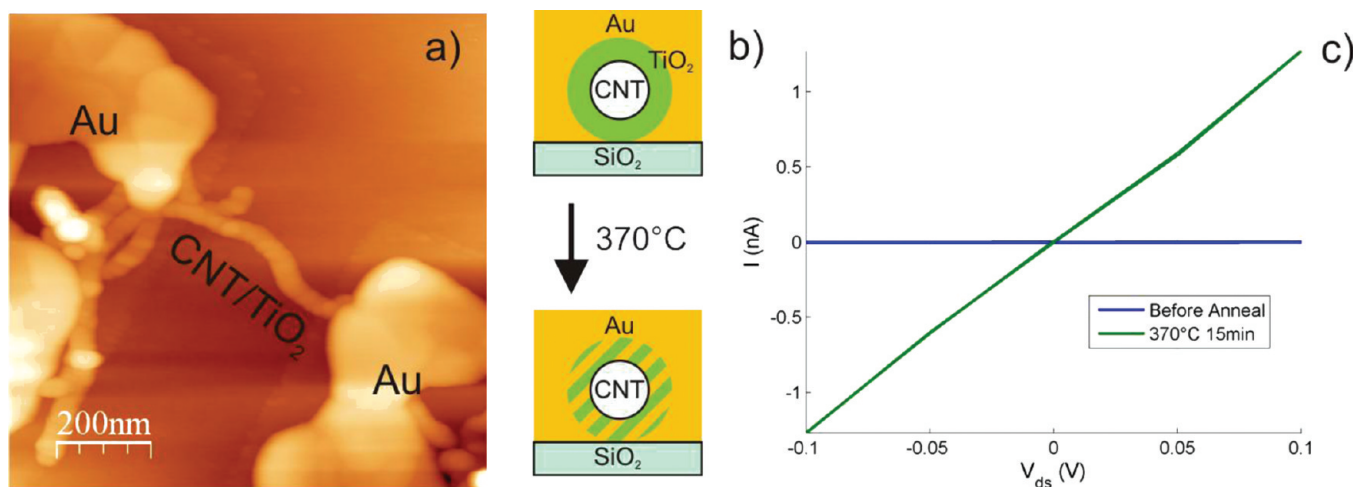


**Figure 6.** (a) AFM image of a single carbon nanotube coated with TiO<sub>2</sub>. The CNT is contacted by two gold contacts which are deformed due to the annealing at 370 °C. (b) Schematic illustration of the alloying procedure to achieve electrical contacts without removing the TiO<sub>2</sub>. (c) Current–voltage measurement before (blue) and after (green) annealing of the device.

TiO<sub>2</sub> coating. Indeed, current–voltage ( $I$ – $V$ ) curves recorded after the annealing (see Figure 6c) reveal a measurable resistance of the order of 100 MΩ. Although the value obtained for the resistance is much larger than typically observed for SWCNTs with two top gold contacts, the results demonstrate the principle feasibility of the approach.

**3.3. Solar Cells.** Different device concepts with the prepared carbon nanostructures incorporated into P3HT/PCBM solar cells were tested within the present work. In a first series of experiments, we followed the common strategy to incorporate CNTs simply as an additive to the BHJ layer. We used multiwalled tubes and functionalized the surface by a treatment with acids. Solutions of as-treated CNTs had a slightly gray color, suggesting that the acid treatment improved the solubility of the CNTs in chlorobenzene, although surface functionalization with acids is mainly expected to increase solubility in polar solvents. Figure 7 shows typical current–voltage curves for a CNT-free reference solar cell as well as for CNT-containing cells. The presented reference solar cell has an open-circuit voltage of 0.56 V, a short-circuit current density of 6.7 mA/cm<sup>2</sup>, a fill factor of 0.48 and a power conversion efficiency of 1.8%. Normal diode-like  $J$ – $V$  curves were obtained. Adding the as-purchased and functionalized CNTs to the BHJ blend resulted in almost ohmic  $J$ – $V$  characteristics (see Figure 7). Obviously, the corresponding solar cells suffer from electrical shorts induced by the relatively long CNTs which are likely to simply connect the electrodes. (Transmission electron microscopy revealed an average length of several micrometers). Therefore, we added a preparative step to shorten the functionalized CNTs. This was done by introducing a sonication step after the treatment with nitric and sulfuric acids (see experimental section for details). The procedure resulted in CNTs with an average length of the order of roughly 200 nm. With shortened CNTs, we were able to obtain diode-like  $J$ – $V$  curves (see Figure 7), but all parameters, the open-circuit voltage ( $V_{OC} \approx 0.43$  V), short-circuit current density ( $J_{SC} \approx 4.0$  mA/cm<sup>2</sup>), fill factor (FF ≈ 0.35), and power conversion efficiency ( $\eta \approx 0.6\%$ ), were reduced in comparison to the reference solar cells. Thus, we could not observe a positive effect of simply adding multiwalled CNTs to the polymer/fullerene blend.

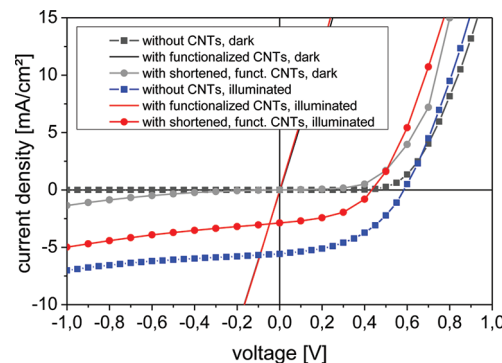


**Figure 7.** Current density–voltage characteristics of P3HT/PCBM solar cells with ITO/PEDOT:PSS and Al as anode and cathode, respectively. A typical CNT-free reference solar cell is compared to solar cells with multiwalled CNTs incorporated into the disordered BHJ layer. The CNTs were functionalized by a treatment with nitric and sulfuric acids, and optionally also shortened by sonication.

Next, we investigated the usability of the CNT arrays on ITO for application in P3HT/PCBM solar cells. Therefore, solar cells with the ITO contact as transparent electrode and an evaporated metal electrode (Al or Au) as opaque top contact were fabricated. Figure 8a shows a schematic illustration of the device architecture. Several modifications of this structure were realized as will be described in the following.

In a first approach, Al was used as top-contact, and the TiO<sub>2</sub> coating was omitted. Figure 8b shows a J–V curve for such a solar cell with an array of ~200 nm long CNTs which was infiltrated with a P3HT:PCBM blend by drop-casting, resulting in ~2 μm thick active layers. In this device configuration, the ITO contact acts as anode and the Al contact acts as cathode, as in the case of the reference solar cell presented in Figure 7. This means that the CNTs, supposed to be metallic, should transport holes to the ITO electrode. This interpretation of the role of the CNTs is in line with the work on disordered blends of multiwalled CNTs, P3HT and PCBM by Berson et al.<sup>21</sup>

As one can see from the  $J$ – $V$  curves in Figure 8b, the device has a poor rectifying behavior and a low parallel resistance. The parallel

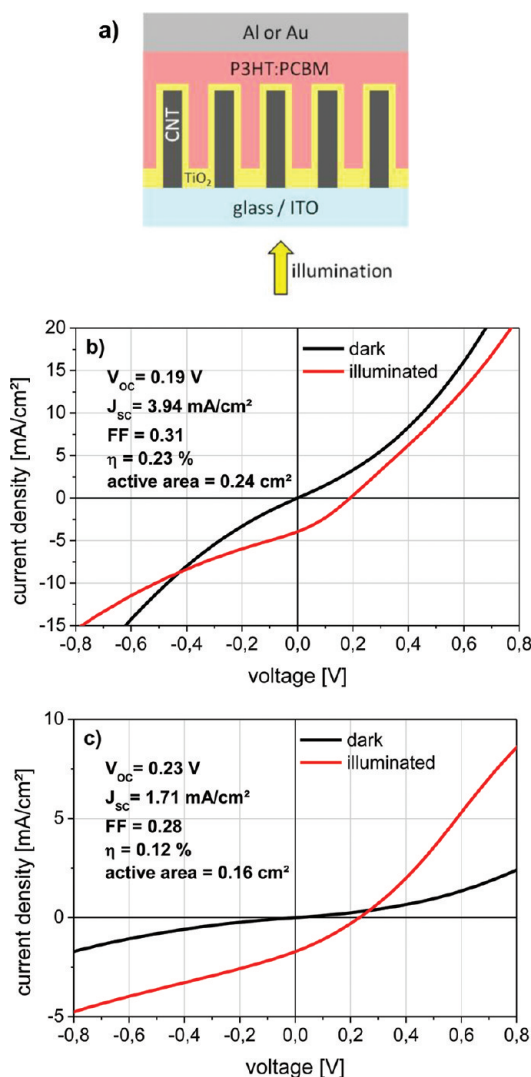


**Figure 8.** (a) Schematic representation of the P3HT/PCBM solar cells with titania-coated CNT arrays on ITO with illumination through the ITO electrode. (b) Current voltage curve of a corresponding solar cell with  $\sim 200$  nm long CNTs, where the titania coating was omitted. The structure was infiltrated by drop-casting with a 1:1 (wt:wt) blend of P3HT:PCBM in chlorobenzene, an annealing step was applied (10 min at  $140^\circ\text{C}$ ), and  $\sim 100$  nm of thermally evaporated Al were used as cathode. (c) Current–voltage curve of a corresponding solar cell with  $\sim 200$  nm long  $\text{TiO}_2$ -coated CNTs. The titania coating was obtained with 6 deposition/annealing steps, the structure was infiltrated by spin-coating with a 1:1 (wt:wt) blend of P3HT:PCBM in chlorobenzene, an annealing step was applied (15 min at  $140^\circ\text{C}$ ), and 50 nm of thermally evaporated Au were used as anode.

resistance can be determined from the slope of the  $J$ – $V$  curves at 0 V following a procedure described in ref 30. Ideally, the parallel resistance should be infinite, and it is usually in the range of at least several  $\text{k}\Omega \cdot \text{cm}^2$  (resistance of the solar cell multiplied by the area) for good organic solar cells.<sup>30</sup> In our case, values of only  $50$ – $60$   $\Omega \cdot \text{cm}^2$  were obtained for both, the dark and illuminated  $J$ – $V$  curves. Nevertheless, a small photoresponse was observed. This demonstrates that the prepared CNT arrays can in principle be used for the incorporation in organic solar cells. The open-circuit voltage, short-circuit current density and fill factor are, however, much lower than in typical organic BHJ solar cells. The best

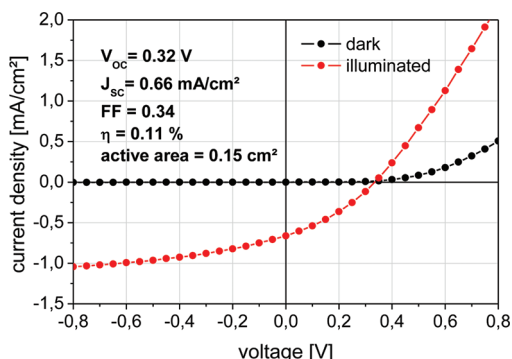


**Figure 9.** Current voltage curve of a solar cell with  $\sim 200$  nm long CNWs without titania coating. The structure was infiltrated by drop-casting with a 1:1 (wt:wt) blend of P3HT:PCBM in chlorobenzene, an annealing step was applied (10 min at  $140^\circ\text{C}$ ), and  $\sim 100$  nm of thermally evaporated Al were used as cathode.

efficiency obtained so far with the presented device concept was only 0.23%.

The low efficiency can be attributed to several factors: (i) First, the device is illuminated from the ITO side, so that the relatively poor transparency of the CNT array is limiting the efficiency. (ii) Second, the low parallel resistance and poor rectifying behavior indicate that despite the average length of  $\sim 200$  nm of the CNTs, there is still a high density of local shunts. Probably, individual tubes with higher length are bridging the electrodes. (iii) The drop-casting technique leads to thick polymer films which helps avoiding shunts. On the other hand, a too thick active layer will, however, hinder efficient charge transport to the Al cathode. (iv) Finally, the CNT array without a selective coating can be considered as an electrode penetrating into the active layer. This should help to efficiently collect holes, but on the other hand increase undesired recombination of electrons at the wrong electrode. Thus, there are several difficulties encountered that limit the performance of this new device concept so far.

A second approach is to use an array of  $\sim 200$  nm long titania-coated CNTs. With an electron-selective coating, at least the problem of undesired recombination should be avoided or reduced. In this case, the CNTs will collect selectively electrons, so that the ITO contact becomes the cathode. Therefore, we used Au as a high work function metal as top contact (anode). This configuration corresponds to so-called inverted organic solar cells.<sup>31–33</sup> Figure 8c shows the  $J$ – $V$  curve for a corresponding solar cell, where the titania-coated CNT array was infiltrated with a P3HT:PCBM blend deposited by spin-coating. A diode-like behavior with improved rectification ratio is found, and the cell shows a clear photoresponse as well. However, also these devices had a low performance so far. The efficiencies obtained were even below those of the devices discussed before. This may be due to the usage of spin-coating instead of drop-casting which results in thinner polymer films. The slope at 0 V indicates a still relatively low parallel resistance ( $R_p = 800 \Omega \cdot \text{cm}^2$  for the dark  $J$ – $V$  curve, and  $R_p = 110 \Omega \cdot \text{cm}^2$  under illumination) which results in a low fill factor of only  $\sim 0.3$ . Probably, also this device suffers from a high density of local shunts which are due to some nanotubes that are still bridging the electrodes. Note that in the case of solar cells prepared with longer CNTs, almost all devices were dominated by electrical shorts which we attribute to the CNTs connecting the electrodes. Furthermore, the difficulty of poor penetration of light through the 200 nm thick CNT array persists, and

we cannot exclude that the titania coating does not perfectly cover the entire surface of the CNTs.

The CNW structures were tested in solar cells as well. Therefore, we prepared devices in analogy to those shown in Figure 8b, i.e., solar cells with  $\sim 100\text{--}200$  nm high CNW structures without  $\text{TiO}_2$  coating and using an Al cathode. Drop-casting was used to infiltrate the CNW structures with P3HT:PCBM blends. Figure 9 shows the J-V characteristics of a corresponding solar cell. These devices show a much better diode-like behavior. The parallel resistance as determined from the slope of the dark  $J\text{--}V$  curve at 0 V is increased to  $R_p = 367 \text{ k}\Omega\cdot\text{cm}^2$ . Under illumination, the value determined for  $R_p$  decreased to  $775 \text{ }\Omega\cdot\text{cm}^2$ , but is still much higher than in the case of the CNT-based solar cells. This results also in a better fill factor of 0.34. These results suggest that the CNW structures are more uniform in height than the CNT arrays, so that the probability to obtain local shunts is decreased. Nevertheless, the open-circuit voltage and short-circuit current density were quite low (see Figure 9). This can be attributed to the still limited penetration of light, the thick organic layer which hinders efficient charge transport to the Al cathode, and to high recombination rates caused by the omitted titania layer.

#### 4. SUMMARY AND CONCLUSIONS

In summary, vertically oriented carbon nanostructures were successfully prepared on ITO substrates by CVD. A static pressure CVD process at relatively low temperature ( $575^\circ\text{C}$ ) enabled obtaining nanotubes with controllable length. Whereas growth times of 10 min resulted in average tube lengths of several micrometers, short growth times enabled restricting the length to about 200 nm. By a plasma-enhanced CVD process, we were able to produce also carbon nanowalls on ITO. Here the height of the walls could also be controlled in the size regime from 100–600 nm.

Furthermore, a procedure was developed to coat the carbon nanostructures with  $\text{TiO}_2$ . In order to verify that titania-coated carbon nanotubes are still good conductors, current–voltage measurements on single carbon nanotubes bridging two contacts were performed.

The prepared carbon nanostructures were investigated with respect to their applicability in organic photovoltaics. Therefore, first test solar cells were fabricated. In some cases, operating solar cells were obtained, but the performance was low, so far. The main difficulties appear to be (i) the occurrence of local shunts due to carbon nanotubes or walls bridging the electrodes, (ii) the limited penetration of light through the carbon nanostructures, (iii) poor charge transport through nonoptimized, thick organic films, and (iv) high recombination rates, when the wrong type of charge carriers reaches the carbon nanostructures. As for the local shunts, solar cells based on the carbon nanowalls showed better diode-like characteristics, suggesting that these structures are more uniform in height than the arrays of carbon nanotubes. As another interesting result we found that titania-coated CNTs can be used as electron collecting electrode (cathode), whereas uncoated CNTs on ITO act as hole collecting electrode (anode).

In conclusion, different carbon nanostructures with small spatial dimensions were successfully developed. According to the first tests performed, these structures appear in principle suitable for application in polymer-based solar cells. However, the solar cells obtained within this work are still far from being optimized, and difficulties were encountered that need to be overcome in future. Optimization strategies for future work may

for example include the usage of transparent grid electrodes as top contact, in order to avoid the difficulty of poor light penetration through the carbon nanostructures.

#### ■ AUTHOR INFORMATION

##### Corresponding Author

\*E-mail address: holger.borchert@uni-oldenburg.de.

#### ■ ACKNOWLEDGMENT

We gratefully acknowledge funding by the Federal Ministry of Education and Research (BMBF, project number 03SF0338). Furthermore, this work was partly supported by the project “EWE Nachwuchsgruppe Dünnschicht-Photovoltaik (Thin Film Photovoltaics)” by the EWE AG, Oldenburg, Germany.

#### ■ REFERENCES

- (1) Thompson, B. C.; Fréchet, J. M. *J. Angew. Chem., Int. Ed.* **2008**, *47*, S8–77.
- (2) Ameri, T.; Dennler, G.; Lungenschmied, C.; Brabec, C. *J. Energy Environ. Sci.* **2009**, *2*, 347–363.
- (3) Deibel, C.; Dyakonov, V. *Rep. Prog. Phys.* **2010**, *73*, 096401.
- (4) Borchert, H. *Energy Environ. Sci.* **2010**, *3*, 1682–1694.
- (5) Park, S. H.; Roy, A.; Beaupre, S.; Cho, S.; Coates, N.; Moon, J. S.; Moses, D.; Leclerc, M.; Lee, K.; Heeger, A. *J. Nat. Photonics* **2009**, *3*, 297–303.
- (6) Liang, Y.; Xu, Z.; Xia, J.; Tsai, S.; Wu, Y.; Li, G.; Ray, C.; Yu, L. *Adv. Mater.* **2010**, *22*, E135–E138.
- (7) Green, M. A.; Emery, K.; Hishikawa, Y.; Warta, W.; Dunlop, E. D. *Prog. Photovolt: Res. Appl.* **2011**, *19*, 565–572.
- (8) Scharber, M. C.; Mühlbacher, D.; Koppe, M.; Denk, P.; Waldlauf, C.; Heeger, A. J.; Brabec, C. *J. Adv. Mater.* **2006**, *18*, 789–794.
- (9) Hoppe, H.; Sariciftci, N. S. *J. Mater. Chem.* **2006**, *16*, 45–61.
- (10) Chen, L.; Hong, Z.; Li, G.; Yang, Y. *Adv. Mater.* **2009**, *21*, 1434–1449.
- (11) Moon, J. S.; Lee, J. K.; Cho, S.; Byun, J.; Heeger, A. *J. Nano Lett.* **2009**, *9*, 230–234.
- (12) van Bavel, S. S.; Sourty, E.; de With, G.; Loos, J. *Nano Lett.* **2009**, *9*, 507–513.
- (13) Oosterhout, S. D.; Wienk, M. M.; van Bavel, S. S.; Thiedmann, R.; Koster, L. J. A.; Gilot, J.; Schmidt, V.; Janssen, R. A. *J. Nat. Mater.* **2009**, *8*, 818–824.
- (14) Robel, I.; Bunker, B. A.; Kamat, P. V. *Adv. Mater.* **2005**, *17*, 2458–2463.
- (15) Kymakis, E.; Kornilios, N.; Koudoumas, E. *J. Phys. D Appl. Phys.* **2008**, *41*, 165110.
- (16) Hu, L.; Zhao, Y.; Ryu, K.; Zhou, C.; Stoddart, F.; Grüner, G. *Adv. Mater.* **2008**, *20*, 939–946.
- (17) Derbal-Habak, H.; Bergeret, C.; Cousseau, J.; Nunzi, J. M. *Sol. Energy. Mater. Sol. Cells* **2011**, *95*, S53–S56.
- (18) Dissanayake, N. M.; Zhong, Z. *Nano Lett.* **2011**, *11*, 286–290.
- (19) Rowell, M. W.; Topinka, M. A.; McGehee, M. D.; Prall, H.; Dennler, G.; Sariciftci, N. S.; Hu, L.; Gruner, G. *Appl. Phys. Lett.* **2006**, *88*, 233506.
- (20) Sgobba, V.; Guldi, D. M. *J. Mater. Chem.* **2008**, *18*, 153–157.
- (21) Berson, S.; de Bettignies, R.; Bailly, S.; Guillerez, S.; Jousselme, B. *Adv. Funct. Mater. Chem.* **2007**, *17*, 3363–3370.
- (22) Liu, J.; Kuo, Y.; Klabunde, K. J.; Rochford, C.; Wu, J.; Li, J. *ACS Appl. Mater. Interfaces* **2009**, *1*, 1645–1649.
- (23) Miller, A. J.; Hatton, R. A.; Chen, G. Y.; Silva, S. R. P. *Appl. Phys. Lett.* **2007**, *90*, 023105.
- (24) Hanprasopwattana, A.; Srinivasan, S.; Sault, A. G.; Datye, A. K. *Langmuir* **1996**, *12*, 3173–3179.
- (25) see for example data at: <http://www.pgo-online.com/intl/katalog/1737.html>.

- (26) Klinke, C.; Waizenegger, C.; Stöckli, T.; Noury, O.; Bonard, J.-M. *AIP Conf. Proc.* **2001**, *591*, 243–246.
- (27) Klinke, C.; Bonard, J.-M.; Kern, K. *Phys. Rev. B* **2005**, *71*, 035403.
- (28) Taguchi, T.; Saito, Y.; Sarukawa, K.; Ohno, T.; Matsumura, M. *New J. Chem.* **2003**, *27*, 1304–1306.
- (29) Sato, T.; Miura, K.; Ishino, N.; Ohtera, Y.; Tamamura, T.; Kawakami, S. *Opt. Quantum Electron.* **2002**, *34*, 63–70.
- (30) Chirvase, D.; Parisi, J.; Hummelen, J. C.; Dyakonov, V. *Nanotechnology* **2004**, *15*, 1317–1323.
- (31) Sahin, Y.; Alem, S.; de Bettignies, R.; Nunzi, J.-M. *Thin Solid Films* **2005**, *476*, 340–343.
- (32) Waldauf, C.; Morana, M.; Denk, P.; Schilinsky, P.; Choulis, S. A.; Brabec, C. *J. Appl. Phys. Lett.* **2006**, *89*, 233517.
- (33) Hau, S. K.; Yip, H.-L.; Baek, N. S.; Zou, J.; O’Malley, K.; Jen, A. K.-Y. *J. Appl. Phys. Lett.* **2008**, *92*, 253301.